Finite viscoelastic modeling of yeast cells with an axisymmetrical shell approach

Z. Awada[a], B. Nedjar[a,*]

[a] *Université Gustave Eiffel, MAST-EMGCU, 5 Boulevard Descartes, 77454 Marne-la-Vallée cedex 2, France*

Abstract

Based on the use of shell kinematics, a theoretical model is developed to predict time-dependent responses of *Saccharomyces cerevisiae* yeasts. These cells are herein described as thin-walled shells with axisymmetrical shapes and, due to their soft nature, the finite strain range is a priori adopted. Accordingly, a finite viscoelastic modeling is assumed for the cell-wall. An Ogden-type energy function is used together with a creep-like potential, this latter to describe the way overstresses vanish at thermodynamic equilibrium. The cell-volume conservation due to the inner incompressible fluid is accounted for via an update procedure of the Uzawa type. Numerical simulations highlight the efficiency of the proposed framework. As a further outcome, the emergence of a necessary cell-wall representation by at least two sets of layers with sensitively different mechanical properties is established.

Keywords: Cell-wall, Axisymmetric shells, Finite viscoelasticity, Internal cell-volume conservation, Finite element method

1. Introduction

Over the past decades, research in the field of cell mechanics has received considerable attention relative to other biomechanical fields. The investigations began experimentally on animal cells around the 1930's. Later on, improvements were made to be able to study the mechanical behaviour of walled cells such as, to mention a few, plant cells, tomato cells, yeast cells, and sea-urchin eggs. In what follows, the interest is on *Saccharomyces cerevisiae* yeasts. This kind of cells plays a crucial role in our lifes as it presents medical, veterinary, economical and cosmetic advantages. The medical, benefits are such as, for example, the production of vitamins, antibiotics and insulin [1]. Economically speaking, yeasts are used in the fabrication of fermented foods and beverages especially bread, wine, beer, among others, e.g. [2, 3]. These cells are in general of spherical, or at least close to spherical shapes, surrounded by a multi-functional wall. Firstly, this latter constitutes a protective barrier against the invasion of bacteria and microbes that can cause infections [4]. It is then essential to understand the disruption process and the extraction of intracellular products [5, 6]. In addition, the wall is primordial to determine the cell shape and to understand its growth [7]. This has been mainly our goal toward the cell-wall characterization and modeling.

During the last years, mathematical models have been initiated with results in [8] on hollow spherical membrane compression together with semi-analytical solution strategies, see [9]. Later on, the modeling has been improved in [5, 10] by representing cells as thin walled, liquid-filled spheres. Several constitutive relationships were assumed for the cell-wall, e.g. Mooney-Rivlin is used in [11, 10] for red blood cells and sea-urchin eggs, respectively. A linear-elastic constitutive relationship for yeast cells has been applied in [5]. Recently, authors in [12] proposed a model by using a Hencky-type law. In reality, there are time-dependent effects such as permeability and intrinsic viscoelasticity of the cell-wall that influence the whole cell response. Those are just few examples of the many models reported in the literature.

In the present contribution, a theoretical and

*Corresponding author, phone: +33 1 81 66 84 16
Email addresses: zeinab.awada@univ-eiffel.fr (Z. Awada), boumediene.nedjar@univ-eiffel.fr (B. Nedjar)

numerical modeling framework is derived for the time-dependent cell response. Yeasts are herein described as axisymmetrical, impermeable, liquid-filled shells. In view of the viscoelastic character of the cell-wall and its soft nature, a finite viscoelastic approach is adopted. The kinematical choice is based on the multiplicative decomposition of the deformation gradient into an elastically relaxing part and a viscous part, e.g. [13, 14]. Use is made of an Ogden-type constitutive relation that we extend toward a finite viscoelastic modeling. In a first approach, we assume that the cell-wall is homogenous, isotropic and incompressible. Furthermore, the internal cell-volume conservation related to the incompressibilty of the fluid is solved via an Uzawa-type update algorithm.

2. Axisymmetric shell modeling

Yeasts can be regarded as thin-walled shell structures and, due to their soft nature, a formulation within the finite strain range is adopted. We first recall the basic kinematics that we extended toward finite viscoelasticity. The balance equation is then given that accounts for the action of the liquid inside a typical closed cell. We next derive the constitutive equations that will be used later on for numerical simulations.

2.1. Finite viscoelastic kinematics

Within the finite strain range, we denote as usual by $\boldsymbol{F}$ the deformation gradient, and we recall the definition of the Green-Lagrange strain tensor $\boldsymbol{E}$ as,

$$\boldsymbol{E} = \frac{1}{2}\left\{\boldsymbol{F}^T\boldsymbol{F} - \mathbf{1}\right\} \ , \tag{1}$$

where $\mathbf{1}$ is the second-order identity tensor. In this study, use is made of the quasi-Kirchhoff-type theory for thin shells of revolution as derived in [15, 16]. The non-zero components of the above strain reduce to the meridional and circumferential ones, here respectively $E_{11} \equiv E_1$ and $E_{22} \equiv E_2$. These latter being regarded as principal strains, the principal stretches λ_γ, $\gamma = 1, 2$, that are relative to the deformation gradient $\boldsymbol{F}$, follow from (1) as,

$$E_\gamma = \frac{1}{2}\big(\lambda_\gamma^2 - 1\big) \ \Rightarrow \ \lambda_\gamma = \sqrt{2E_\gamma + 1} \ , \tag{2}$$

together with $\lambda_3 = 1$.

Now for the extension toward finite viscoelasticity, use is made in this work of the multiplicative decomposition of the deformation gradient $\boldsymbol{F}$ into an elastically relaxing part $\boldsymbol{F}^{\mathrm{e}}$ and a viscous part $\boldsymbol{F}^{\mathrm{v}}$, e.g. see [14, 17]: $\boldsymbol{F} = \boldsymbol{F}^{\mathrm{e}}\boldsymbol{F}^{\mathrm{v}}$, and that we adapt to the present shell theory. A multiplicative decomposition of the stretches is then deduced as well,

$$\lambda_i = \lambda_i^{\mathrm{e}}\lambda_i^{\mathrm{v}} \ , \tag{3}$$

where λ_i^{e} and λ_i^{v} are the principal stretches relative to $\boldsymbol{F}^{\mathrm{e}}$ and $\boldsymbol{F}^{\mathrm{v}}$, respectively. For later use, we define the logarithmic strains of the above stretches as,

$$\varepsilon_i = \ln\lambda_i \ , \quad \varepsilon_i^{\mathrm{e}} = \ln\lambda_i^{\mathrm{e}} \ , \quad \varepsilon_i^{\mathrm{v}} = \ln\lambda_i^{\mathrm{v}} \ , \tag{4}$$

and, further, the multiplicative decomposition implies,

$$\varepsilon_i = \varepsilon_i^{\mathrm{e}} + \varepsilon_i^{\mathrm{v}} \ . \tag{5}$$

2.2. Mechanical balance

Within a Lagrangian formulation, the mechanical balance of a yeast cell that occupies the domain $\mathcal{B}$ in its reference configuration can be given in terms of the second Piola-Kirchhoff stress tensor $\boldsymbol{S}$ by the following weak form:

$$\int_{\mathcal{B}} \boldsymbol{S} : \delta\boldsymbol{E} \ \mathrm{d}V = -\int_{\partial\mathcal{B}_t} \hat{p}\boldsymbol{n}.\delta\boldsymbol{u} \ \mathrm{d}a \ , \qquad \forall\delta\boldsymbol{u} \ , \tag{6}$$

where $\delta\boldsymbol{u}$ is a variation of the displacement field $\boldsymbol{u}$. Here we consider follower loads $\hat{p}\boldsymbol{n}$ acting in the direction $\boldsymbol{n}$ normal to the deformed shell $\mathcal{B}_t$, and the integration of which is more easily performed with respect to the current configuration, [18, 19] among others. For an axisymmetric quasi-Kirchhoff shell of mid-surface reference $\mathcal{M}$ and thickness h, Eq. (6) is rewritten as,

$$2\pi\left\{\int_{\mathcal{M}}\int_h S_\gamma\delta E_\gamma \, r\mathrm{d}\xi\mathrm{d}s + \epsilon\int_{\mathcal{M}}\int_h E_{13}\delta E_{13} \, r\mathrm{d}\xi\mathrm{d}s\right\} = -\int_{\partial\mathcal{B}_t} \hat{p}\boldsymbol{n}.\delta\boldsymbol{u} \ \mathrm{d}a, \tag{7}$$

with $\xi \in [-h/2, +h/2]$, and where ϵ is the penalty parameter for the transverse shear part, i.e. the constraint $E_{13} = 0$. Accordingly, S_γ are the principal second Piola-Kirchhoff stresses that are work conjugate with the principal strains E_γ, $\gamma = 1, 2$.

In what follows, the constitutive equations will be given in terms of the Kirchhoff stress tensor $\boldsymbol{\tau}$ that is related to $\boldsymbol{S}$ by the push-forward procedure $\boldsymbol{\tau} = \boldsymbol{F}\boldsymbol{S}\boldsymbol{F}^T$. One has the following connection:

$$S_\gamma = \frac{\tau_\gamma}{\lambda_\gamma^2} \ , \tag{8}$$

where τ_γ are principal Kirchhoff stresses.

2.3. Constitutive equation: finite viscoelasticity

Motivated by the generalized Maxwell model, see Fig. 1, the free energy ψ is additively split into an equilibrium part $\psi_{\rm eq}$, and a non-equilibrium part $\psi_{\rm neq}$. While the former depends on the total strains, the latter depends on the elastically relaxing ones. Herein, we choose the following incompressible N=1-Ogden-type model written in terms of principal stretches as,

$$\begin{aligned}\psi &= \underbrace{\frac{2\mu}{\alpha^2}\Big(\lambda_1^\alpha+\lambda_2^\alpha+\lambda_3^\alpha-3\Big)}_{\psi_{\rm eq}} \\ &+ \underbrace{f\frac{2\mu}{\alpha^2}\Big(\lambda_1^{{\rm e}\,\alpha}+\lambda_2^{{\rm e}\,\alpha}+\lambda_3^{{\rm e}\,\alpha}-3\Big)}_{\psi_{\rm neq}}\,,\end{aligned} \tag{9}$$

where μ denotes the *long-term* shear modulus, α the Ogden's coefficient, and the adimensional factor f is a weighting parameter for the overstress contribution, i.e. the instantaneous shear modulus is here evaluated as $(1+f)\mu$. A Neo-Hooke-type model is retrieved with $\alpha=2$. Notice that other choices instead of the form (9) can be used as well, e.g. [20, 21].

Next, the principal Kirchhoff stresses are given by,

$$\tau_i = \lambda_i\frac{\partial\psi_{\rm eq}}{\partial\lambda_i}+\lambda_i^{\rm e}\frac{\partial\psi_{\rm neq}}{\partial\lambda_i^{\rm e}}+\varsigma, \tag{10}$$

where ς denotes the pressure related to the material incompressibility. It is deduced from the plane stress assumption $\tau_3=0$, and when replaced back into Eq. (10), we end-up with the following constitutive relation for the present axisymmetric shell theory:

$$\tau_\gamma = \underbrace{\frac{2\mu}{\alpha}\Big(\lambda_\gamma^\alpha-(\lambda_1\lambda_2)^{-\alpha}\Big)}_{\tau_{{\rm eq}\gamma}}+\underbrace{f\frac{2\mu}{\alpha}\Big(\lambda_\gamma^{{\rm e}\,\alpha}-(\lambda_1^{\rm e}\lambda_2^{\rm e})^{-\alpha}\Big)}_{\tau_{{\rm neq}\gamma}}, \tag{11}$$

for $\gamma=1,2$.

In parallel, it is crucial to develop the way the non-equilibrium stress $\boldsymbol{\tau}_{\rm neq}$ vanishes at thermodynamic equilibrium. The dissipation related to viscoelasticity is given by, e.g. [14, 22, 19] :

$$\mathcal{D} = \boldsymbol{\tau}_{\rm neq}:\left[-\frac{1}{2}\Big(\pounds_v\boldsymbol{b}^{\rm e}\Big)\boldsymbol{b}^{{\rm e}^{-1}}\right]\geq 0\,, \tag{12}$$

where

$$\pounds_v\boldsymbol{b}^{\rm e} = \boldsymbol{F}\left[\frac{{\rm d}\boldsymbol{C}^{{\rm v}^{-1}}}{{\rm d}t}\right]\boldsymbol{F}^T \tag{13}$$

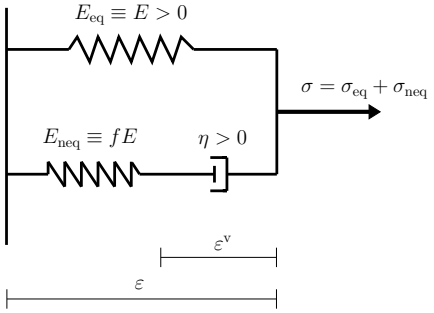

Figure 1: Motivation: one-dimensional generalized Maxwell model.

is the Lie derivative of the elastically relaxing left Cauchy-Green tensor $\boldsymbol{b}^{\rm e}=\boldsymbol{F}^{\rm e}\boldsymbol{F}^{{\rm e}^T}\equiv\boldsymbol{F}\boldsymbol{C}^{{\rm v}^{-1}}\boldsymbol{F}^T$, and where $\boldsymbol{C}^{\rm v}=\boldsymbol{F}^{{\rm v}^T}\boldsymbol{F}^{\rm v}$ is the viscous right Cauchy-Green tensor.

A simple way to satisfy the inequality (12) for any admissible process is to postulate the existence of a creep-like potential that we denote here by $\phi_{\rm vis}(\boldsymbol{\tau}_{\rm neq})$, a convex function such that,

$$-\frac{1}{2}\Big(\pounds_v\boldsymbol{b}^{\rm e}\Big)\boldsymbol{b}^{{\rm e}^{-1}} = \frac{\partial\phi_{\rm vis}(\boldsymbol{\tau}_{\rm neq})}{\partial\boldsymbol{\tau}_{\rm neq}}\,. \tag{14}$$

Further, convenient for the present formulation, $\phi_{\rm vis}$ is equivalently expressed in terms of principal stresses; $\phi_{\rm vis}(\boldsymbol{\tau}_{\rm neq})\equiv\hat{\phi}_{\rm vis}(\tau_{{\rm neq}_1},\tau_{{\rm neq}_2})$, and to make matters as concrete as possible, the following quadratic form will be used in the present work,

$$\hat{\phi}_{\rm vis} = \frac{1}{2\eta}\Big(\tau_{{\rm neq}_1}^2+\tau_{{\rm neq}_2}^2\Big), \tag{15}$$

where η is the viscosity parameter such that the associated relaxation time τ is given by,

$$\tau = \frac{\eta}{f\mu}\,. \tag{16}$$

When written in principal components, and taking into account (15), the tensorial form (14) of the evolution equation becomes,

$$\dot{\varepsilon}_\gamma^{\rm v} = \frac{\tau_{{\rm neq}_\gamma}}{\eta}\qquad\gamma=1,2\,, \tag{17}$$

and the numerical resolution of which is nowadays classical, e.g. [14, 23, 19].

Thus, in *summary*, four mechanical parameters are needed to identify the cell-wall viscoelastic behaviour: (i) the long-term shear modulus μ, (ii)

the N=1-Ogden coefficient α, (iii) the adimensional factor that characterizes the level of the non-equilibrium overstresses f, and (iv) the relaxation time of the viscous evolution τ.

3. Intrinsic cell-wall parameters

Few studies have reported time-dependent mechanical properties of yeast cell-walls, most probably because of the difficulties related to the cellular dimensions. Here in the absence of an ad-hoc experimental campaign which would have made it possible to carry out a method to identify the material parameters, use is made of direct results found in [24], see also [25]. So far, it is noticiable that too few results have been reported in the literature on measuring viscoelastic properties of single yeast cells.

The key point is that, as for any model within the finite strain range, the one of Section 2.3 tends to its *linear* viscoelastic version at the limiting case of an infinitesimal perturbation. This property is here exploited accordingly. Thereby, the rheological model of Fig. 1 is nowadays classical and its apparatent Young modulus is given by,

$$E^\star = E(1 + f e^{-\frac{t}{\tau}}), \tag{18}$$

from whichone can identify the long- and short-term moduli E and $(1+f)E$, respectively, in complete agreement with the constitutive relation (11).

In the reference [24], the values found for the short-term modulus were about $3.67 \pm 0.27\,\text{MPa}$, while for the long-term modulus, they were about $1.16 \pm 0.22\,\text{MPa}$. The relaxation time was about 6 to 7 s. Observe that the diversity of some viscoelastic properties may depend, on several biological factors such as, growth phases, biological culture, and so on. Hence, with regards to the expression (18), this gives the following estimates within the present framework:

$$\begin{aligned} E &= 1.16 \pm 0.22\,\text{MPa}, \\ f = 2.325 \pm 0.865, &\quad \tau = 6.5 \pm 0.5\,\text{s}. \end{aligned} \tag{19}$$

Further, interesting observations must be pointed-out at this stage: (i) the relaxation time τ is of the order of few seconds, (ii) the overstress factor f is far from negligible, i.e. here about 230%, and (iii) whether the long- or short-term moduli, their values are in the range of earlier reported Young moduli, as in [7, 26], but different by two orders of magnitude from values acquiered by other authors, for instance in [27, 12]. This point will be brought up and discussed again in Section 5.1.1.

4. Internal cell-volume conservation during loading

Inside the closed cell, the liquid resists to the applied outer loads. It is represented by a normal pressure on the inner surface. Thus, focus is made on the external surface load term in Eq. (7) that we rewrite here for the sake of clarity:

$$g_p(\boldsymbol{u}, \delta\boldsymbol{u}) = -\int_{\partial\mathcal{B}_t} \delta\boldsymbol{u}.\hat{p}\boldsymbol{n}\ \mathrm{d}a\ , \tag{20}$$

where the deformation-dependent unit normal vector $\boldsymbol{n}$ is chosen pointing toward the interior of the cell. The pressure magnitude $\hat{p}$ can increase or decrease due to the conserved cell-volume during compression as the filled liquid is taken to be incompressible: $\hat{p}$ constitutes then an additional unknown of the problem at hand. We propose in this section a method to numerically solve for it.

Let denote by V_{int_0} the initial volume inside the cell. During a *global* iterative process, say at iteration (k) where the mechanical equilibrium is solved with a fixed current estimate of the internal pressure $\hat{p}^{(k)}$, one computes the resulting internal volume $V_{\text{int}}^{(k)}$ within the post-processing. Then, if $V_{\text{int}}^{(k)} < V_{\text{int}_0}$, the pressure amplitude must be increased, while it must be decreased if $V_{\text{int}}^{(k)} > V_{\text{int}_0}$. Herein, this update procedure is encompassed by the following Uzawa-like algorithm,

$$\hat{p}^{(k+1)} = \hat{p}^{(k)} + \varpi\Big(1 - \frac{V_{\text{int}}^{(k)}}{V_{\text{int}_0}}\Big), \tag{21}$$

where ϖ is a penalty parameter.

5. Numerical simulations

In this set of simulations, we consider examples where yeasts are compressed between parallel flat plates. The first example treats the classical case of spherical cells with noteworthy observations. Then, pushing further the possibilities of the present framework, a non spherical geometry is considered in a second example.

5.1. Compressions of a spherical yeast

We consider a spherical yeast of external diameter 5 µm and thickness $h = 150$ nm. The initial mid-plane diameter is then $D = 4.85$ µm. For the finite element simulations, 200 shell elements are used. The (rigid) plates are modeled by implicit functions. A frictionless contact is adopted through a penalty formulation, see for example [18]. For the cell-wall, we use the set of parameters (19) together with Ogden's coefficient $\alpha = 4$:

$$\mu = 0.39\,\text{MPa},\ \alpha = 4,\ f = 2.325,\ \tau = 6.5\,\text{s}. \quad (22)$$

Fig. 2 presents the results of computations at different compression speeds: *(i)* very slow, *(ii)* very fast, and *(iii)* at intermediate velocities of 0.4 and 2 µm/s. The reaction forces are plotted versus the fractional deformations z/D, where z is the downward vertical displacement of the upper plate. Notice the consequence of the cell-wall viscoelasticy on the time-dependent response of the whole cell.

In parallel, to show the efficiency of the nested algorithm derived in Section 4, the corresponding evolutions of the relative internal volumes are shown in Fig. 3. For all the computations, they at most deviate at less than 0.15% of the initial internal volume V_{int_0}. Finally, and for illustrative purposes, Fig. 4 shows typical deformed configurations at different compression levels, here for the case of the compression at the velocity of 2 µm/s.

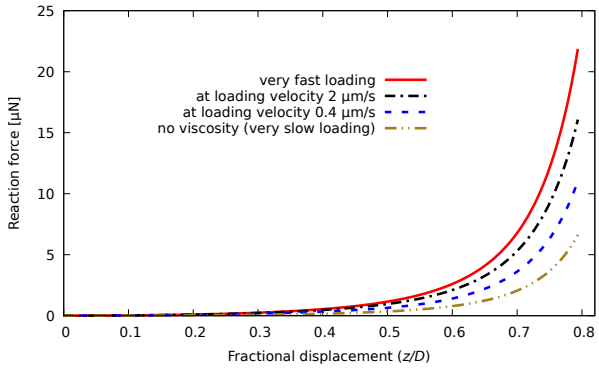

Figure 2: Compression of a spherical cell at different loading velocities.

5.1.1. Comments and discussions

Even if the shapes of the curves in Fig. 2 are qualitatively in good agreement with those found in the literature, quantitatively this is not the case. The reaction forces are here lower by at least one order of magnitude from values obtained in, e.g. [27, 28]. The reason is most probably because, so far, we have supposed the cell-wall as homogeneous. However, the biological composition of S. cerevisiae cell-wall is nowadays well understood. Its two major components are β-glucan and mannoproteins which respectively represent about 50-60% and 40-50% of the cell-wall mass, see [7]. A third component is the chitin that, even at low amounts (1-3%), has stiff mechanical properties. From the modeling point of view, it would be reasonable to represent the cell-wall as layered through its thickness, with at least two sets of layers: (i) a soft outer layer mostly made

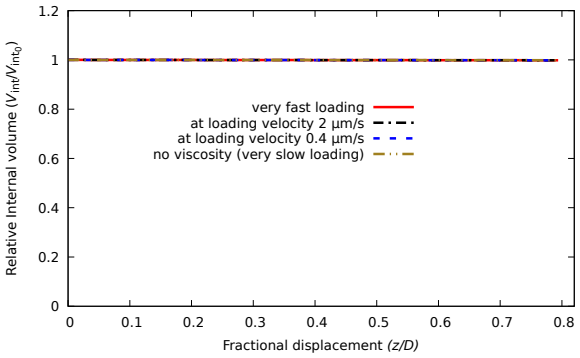

Figure 3: Internal cell-volume variations for the different loading velocities.

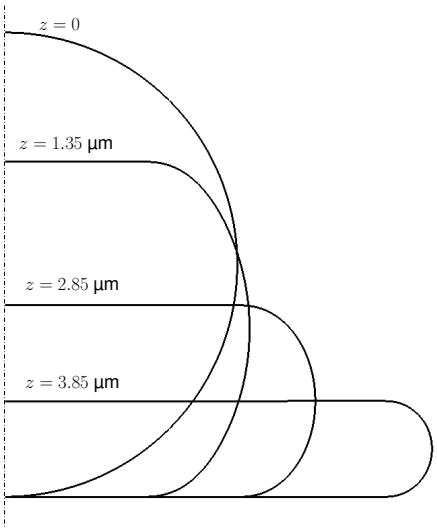

Figure 4: Initial and different deformed configurations of the spherical cell for the compressive loading at 2 µm/s.

of mannoproteins, and (*ii*) and a stiff inner layer mostly made of β-glucan and chitin.

Indeed, and as it was demonstrated in [29] for elasticity, while AFM puts to contribution the soft part of the cell-wall, micromanipulation mostly puts to contibution its stiffer part. For illustrative purposes, Fig. 5 shows results of similar computations as for Fig. 2, but this time with the following material parameters though the cell-wall thickness:

$$\begin{aligned} \mu &= 0.39\,\text{MPa}, \qquad \text{for } \xi \in [0, \frac{h}{2}], \\ \mu &= 39\,\text{MPa}, \qquad \text{for } \xi \in [-\frac{h}{2}, 0], \end{aligned} \tag{23}$$

that is, with a long-term modulus two orders higher in magnitude for the inner half wall, see [5, 28]. The rest of the viscoelastic parameters are kept identical due to the lack of informations: $\alpha = 4$, $f = 2.325$, and $\tau = 6.5\,\text{s}$. Here one can observe that, quantitatively, the levels of reaction forces are of the order of those obtained in [27, 12].

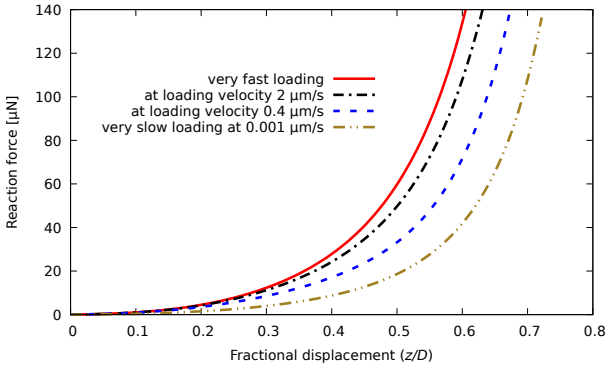

Figure 5: Compression of a layered spherical cell at different loading velocities.

5.2. *Compression of ellipsoidal yeasts*

In this last example, we consider an ellipsoidal yeast cell with a prolate spheroid shape. The initial mid-plane is of major diameter $D = 4.85$ µm and minor diameter $d = 3$ µm, and the wall thickness is taken as $h = 150$ nm. For the finite element simulations, 100 shell elements are used, and the compression between the flat plates is here again modeled by frictionless contact with implicit functions. For the cell-wall, we use the above two-layers model, this time with a Neo-Hooke-type model:

$$\begin{aligned} \mu &= 0.39\,\text{MPa}, \qquad \text{for } \xi \in [0, \frac{h}{2}], \\ \mu &= 39\,\text{MPa}, \qquad \text{for } \xi \in [-\frac{h}{2}, 0], \end{aligned} \tag{24}$$

together with $\alpha = 2$, $f = 2.325$, and $\tau = 6.5\,\text{s}$ for both layers.

Fig. 6 presents the results of computations at different compression speeds: *(i)* very slow at 0.001 µm/s, *(ii)* very fast, and *(iii)* at intermediate velocities of 1 and 2 µm/s. The reaction forces are plotted versus the fractional deformations z/D, where z is the downward vertical displacement of the upper plate. Notice here again the consequence of the cell-wall viscoelasticity on the time-dependent response of the whole cell. In the end, Fig. 7 shows typical deformed configurations at different compression levels, here once more for the case of the compression at the velocity of 2 µm/s.

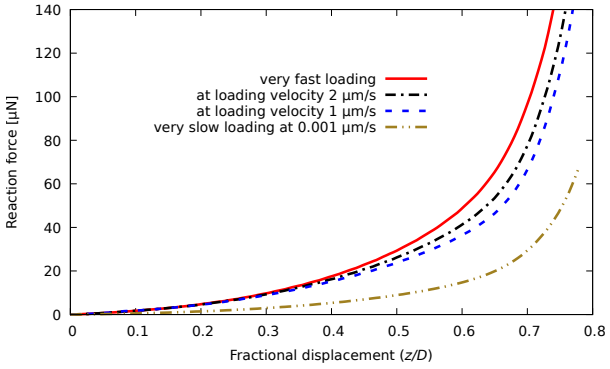

Figure 6: Compression of an ellipsoidal cell at different loading velocities.

6. Conclusions and perspectives

The aim of this contribution was to derive a viscoelastic modeling framework within the finite strain range that is adapted for the modeling of S. cerevisiae yeast cells. Within a shell theory approach, an Ogden-type model has been proposed. The viscoelastic part is motivated by the generalized Maxwell model in conjunction with a multiplicative decomposition of the deformation gradient. An internal variable approach has then been adopted, the evolution of which satisfies the continuum thermodynamics requirements.

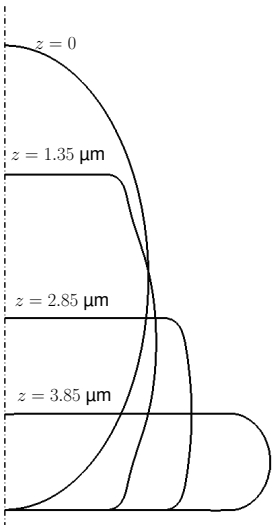

Figure 7: Initial and different deformed configurations of the ellipsoidal cell for the compressive loading at 2 µm/s.

Further, the very important internal cell-volume conservation is taken into account as well. For this, we have derived a nested algorithmic strategy in conjunction with an Uzawa-like update procedure to adjust the amplitudes of the unknown follower pressure. The numerical simulations have shown the ability of the present framework to predict the responses under different loading situations and at various speeds.

We believe that this framework can trigger deeper research. For instance, this modeling can be used to capture the influence of the culture conditions on the mechanical responses. Further, an extension toward general shells will increase the field of applications, i.e. for any cell geometries.

Acknowledgement

The authors would like to thank the french ANR agency for the financial support within the frame of Rheolife project (ANR-18-CE45-0012).

References

[1] R. Hatoum, S. Labrie, I. Fliss, Antimicrobial and probiotic properties of yeasts: From fundamental to novel applications, Frontiers in Microbiology **3** (2012) 421.

[2] C. Lahue, A. A. Madden, R. R. Dunn, C. S. Heil, History and domestication of saccharomyces cerevisiae in bread baking, Frontiers in Genetics **11** (2020) 1373.

[3] M. Parapouli, A. Vasileiadis, A. S. Afendra, E. Hatziloukas, Saccharomyces cerevisiae and its industrial applications, AIMS Microbiology **6**(1) (2020) 1–31.

[4] E. Moeendarbary, E. Harris, Cell mechanics: principles, practices, and prospects, WIREs Systems of Biology and Medicine **6** (2014) 371–388.

[5] A. E. Smith, Z. Zhang, C. R. Thomas, K. E. Moxham, A. P. J. Middelberg, The mechanical properties of saccharomyces cerevisiae, Proceedings of the National Acadaemy of Sciences of the United States of America **97** (2000) 9871–9874.

[6] H. Mashmoushy, Z. Zhang, C. R. Thomas, Micromanipulation measurement of the mechanical properties of baker's cells, Biotechnology Techniques **12**(12) (1998) 925–929.

[7] E. Dague, R. Bitar, H. Ranchon, F. Durand, H. Martin Yken, J. M. François, An atomic force microscopy analysis of yeast mutant defective in cell wall architecture, Yeast **27** (2010) 673–684.

[8] W. W. Feng, W. H. Yang, On the contact problem of an inflated spherical nonlinear membrane, Journal of Applied Mechanics **40** (1973) 209–214.

[9] C. X. Wang, L. Wang, C. R. Thomas, Modelling the mechanical properties of single suspension-cultured tomato cells, Annals Botany **93** (2004) 443–453.

[10] T. J. Lardner, P. Pujara, Compression of spherical cells, Mechanics Today **5** (1980) 161–176.

[11] R. Skalak, A. Tozeren, R. P. Zarda, S. Chien, Strain energy function of red blood cell membranes, Biophysical Journal **13** (1973) 245–263.

[12] J. D. Stenson, C. R. Thomas, P. Hartley, Modelling the mechanical properties of yeast cells, Chemical Engineering Science **64** (2009) 1892–1903.

[13] J. Sidoroff, Un modèle viscoélastique non linéaire avec configuration intermédiaire, Journal de Mécanique **13** (1974) 679–713.

[14] S. Reese, S. Govindjee, A theory of finite viscoelasticity and numerical aspects, International Journal of Solids and Structures **35**(26-27) (1998) 3455–3482.

[15] W. Wagner, A finite element model for non-linear shells of revolution with finite rotations, International Journal for Numerical Methods in Engineering **29** (1990) 1455–1471.

[16] P. Wriggers, R. Eberlein, F. Gruttman, An axisymmetrical quasi-Kirchhoff shell element for large plastic deformations, Archive of Applied Mechanics **65** (1995) 465–477.

[17] B. Nedjar, An anisotropic viscoelastic fibre-matrix model at finite strains: Continuum formulation and computational aspects, Computer Methods in Applied Mechanics and Engineering **196** (2007) 1745–1756.

[18] P. Wriggers, Nonlinear Finite Element Methods, Springer-Verlag, Berlin, Heidelberg, 2008.

[19] B. Nedjar, A coupled BEM-FEM method for finite strain magneto-elastic boundary-value problems, Computational Mechanics **59** (2017) 795–807.

[20] P. Steinmann, M. Hossain, G. Possart, Hyperelastic models for rubber-like materials: consistent tangent operators and suitability for Treloar's data, Archive of Applied Mechanics **82** (2012) 1183–1217.

[21] B. Nedjar, H. Baaser, R. J. Martin, P. Neff, A finite element implementation of the isotropic exponentiated Hencky-logarithmic model and simulation of the eversion of elastic tubes, Computational Mechanics **62**(4)

(2018) 635–654.
[22] B. Nedjar, Frameworks for finite strain viscoelastic-plasticity based on multiplicative decompositions. Part I: Continuum formulations, Computer Methods in Applied Mechanics and Engineering **191** (2002) 1541–1562.
[23] B. Nedjar, Frameworks for finite strain viscoelastic-plasticity based on multiplicative decompositions. Part II: Computational aspects, Computer Methods in Applied Mechanics and Engineering **191** (2002) 1563–1593.
[24] M. R. Ahmad, M. Nakajima, S. Kojima, M. Homma, T. Fukuda, Nanoindentation methods to measure viscoelastic properties of single cells using sharp, flat, and buckling tips inside ESEM, IEEE Transactions on nanobioscience **9**(1) (2010) 12–23.
[25] T. Fukuda, F. Arai, M. Nakajima, Micro-Nanorobotic Manipulation Systems and Their Applications, Springer-Verlag, Berlin Heidelberg, 2013.
[26] B. Goldenbogen, W. Giese, M. Hemmen, J. Uhlendorf, A. Herrmann, E. Klipp, Dynamics of cell wall elasticity pattern shapes during yeast mating morphogenesis, Open Biology **6** (2016) 160136.
[27] A. E. Smith, K. E. Moxham, A. P. J. Middelberg, On uniquely determining cell-wall material properties with the compression experiment, Chemical Engineering Science **53** (1998) 3913–3922.
[28] J. D. Stenson, P. Hartley, C. Wang, C. R. Thomas, Determining the mechanical properties of yeast cell walls, Biotechnology Progress **27** (2011) 505–512.
[29] R. Mercadé-Prieto, C. R. Thomas, Z. Zhang, Mechanical double layer model for Saccharomyces Cerevisiae cell wall, European Biophysics Journal **42** (2013) 613–620.